Triple-differential cross section for the twisted-electron-impact ionization of the water molecule

Nikita Dhankhar and R. Choubisa*

Department of Physics, Birla Institute of Technology and Science-Pilani, Pilani Campus, Pilani, Rajasthan, 333031, India

(Received 2 August 2021; accepted 3 May 2022; published 2 June 2022)

In this paper, we present the results of the triple differential cross section (TDCS) for the (e, 2e) process on H_2O molecule for the plane wave and the twisted electron beam impact. The formalism is developed in the first Born approximation. We describe the plane or twisted wave, plane wave, the linear combination of atomic orbitals (LCAO) (self-consistent field LCAO method), and Coulomb wave for the incident electron, scattered electron, the molecular state of H_2O, and the ejected electron, respectively. We investigate the angular profiles of the TDCS for the outer orbitals $1b_1$, $3a_1$, $1b_2$, and $2a_1$ of the water molecule. We compare the angular profiles of the TDCS for the different values of orbital angular momentum (OAM) number m of the twisted electron beam with that of the plane wave beam. We also study the TDCS for macroscopic H_2O target to explore the effect of opening angle θ_p of the twisted electron beam on the TDCS. Our results clearly show the effect of the twisted electron's OAM number (m) and the opening angle θ_p on the TDCS of the water molecule.

DOI: 10.1103/PhysRevA.105.062801

I. INTRODUCTION

One of the most important collision processes in atomic and molecular physics is the ionization of a given target by an electron impact [hereafter referred as an (e, 2e) process]. In a coincident (e, 2e) process, the interaction of the incident electron leads to the ionization of the target. The ejected and the scattered electrons are detected with their angles and momenta fully resolved [1]. The study of a coincident (e, 2e) process in different kinematical domains is important for investigating the collision dynamics. The (e, 2e) study also helps in probing electron correlation and the structure of a given target [2]. The electron impact ionization studies of atoms and molecules have applications in other fields, e.g., astrophysics, lasers, plasma physics, and radiation physics. The triple differential cross section (TDCS) provides detailed information about an (e, 2e) process and can be defined as the probability of detecting the outgoing electrons in coincidence with their momenta fully resolved. The exploration of TDCS for different atomic and molecular targets has progressed significantly with experimental and reliable theoretical results [2–10].

The water molecule plays a crucial role in biological matters. The study of ionization of water molecule is valuable in radiology, radiation treatment, and planetary atmosphere [11–13]. To dig into the finer aspects of charged particle interactions in a biological medium, the study of ionizing processes by electron impact for water molecules is important. The calculation of differential cross sections for the molecular (e, 2e) process is challenging when compared to that for the atomic (e, 2e) process because of the complex molecular configurations and the orientation dependency of the molecule. In literature, various theoretical models have been employed for the study of (e, 2e) processes on water molecule. Champion *et al.* [14] used different models, such as the one Coulomb wave (1CW) (using the partial wave expansion method), the distorted wave Born approximation (DWBA), the Brauner Briggs Klar (BBK), the two Coulomb wave (2CW), and the dynamic screening of the three two-body Coulomb interactions (DS3C), to study the (e, 2e) process on H_2O molecule. 1CW model with Gaussian-type orbitals (GTO) has also been used to study the TDCS [15]. Different other models, such as 1CW (analytical expression) [16,17], generalized Sturmian function (GSF) [18], two molecular three-body distorted wave approach (M3DW) [19], multicenter three distorted waves (MCTDW) [20], second-order distorted wave Born approximation (DWBA2) [21], have also been used. In addition to (e, 2e) processes, various theoretical (e, 3e) investigations have been done to study the double ionization on H_2O [22–24].

So far, only plane wave electron beams (with no intrinsic orbital angular momentum (OAM)) have been used to study the (e, 2e) collision experiments on H_2O. The experimental realization of electron vortex beams (also known as twisted electron beams, carrying an additional OAM) by different groups ushered in a new era of research into investigating the interactions of atomic and molecular targets with twisted electron beams [25–27]. The term "vortex beam" here refers to a freely propagating electron beam having a helical wave front and a well-defined OAM, m, along the propagation direction. These beams have a helical phase front $e^{im\phi}$ with the azimuthal angle ϕ about the propagation axis (for more details about EVBs, see Refs. [28–30]). The characteristics of the twisted electron beam, such as quantized OAM along their propagation direction, helical structure, and transverse momentum, helps us to understand finer aspects of the twisted electron atom or molecule interactions, which are distinct from the studies reported with the conventional untwisted electron beams explored so far. The study of ionization cross section by twisted electron beams is helpful in

*rchoubisa@pilani.bits-pilani.ac.in

obtaining information about the structure of target, such as characterization of chiral enantiomers [29,31]. The study of twisted electron cross sections is useful in controlling the electron emission angle, improving the image resolutions in electron microscopy [27,32]. The angular profiles of the differential cross section by Harris *et al.* [33] and Dhankhar *et al.* [34,35] show that the TDCS for a twisted electron beam are significantly different from the plane wave cross section. These studies open an avenue for the exploration of experimental setup and further theoretical studies with more sophisticated methods for the twisted electron beams. Twisted electron beams also provide scope for research in optical microscopy, quantum state manipulation, optical tweezers, astronomy, strong-field ionization, and many more fields [26,36–38].

The intrinsic angular momentum of the electron vortex beam influences the role of an electron in the ionization process [39]. Therefore, it is essential to understand the interaction of electron beam, with nonzero OAM, at atomic or molecular level to explore their applications to other fields. Theoretical descriptions of radiative recombination, elastic scattering, impact ionization, and impact excitation have been investigated so far. The work by Ivanov and Serbo [40], Boxem *et al.* [41,42] contributed to the outset of the theoretical analysis of the scattering experiments by twisted electrons. Serbo *et al.* [43] analyzed the scattering by twisted electrons in the relativistic framework. Schüler and Berakdar theoretically investigated the electron energy-loss spectroscopy (EELS) for the C_{60} fullerene target [44] by a twisted electron beam. Karlovets *et al.* [45] studied the scatterig in the framework of Born approximation. Maiorova *et al.* [46] advanced the scattering studies by their theoretical analysis of the differential cross section (DCS) for the elastic scattering of twisted electrons by molecular hydrogen H_2. The angular distribution of the DCS highlighted the influence of the twisted electron beam's parameter on the Young-type interference. Harris *et al.* reported the ionization of the Hydrogen atom by twisted electrons by analyzing the fully differential cross section (FDCS) with different parameters of the twisted electron beam [33]. The results indicated a shift in the binary and recoil peak for twisted electron cross sections from their plane wave locations due to the projectile's transverse momentum components. The recent study by Mandal *et al.* showed the dependence of the total angular momentum (TAM) number (m), and opening angle (θ_p) on the angular profile of the TDCS and spin asymmetry for the relativistic electron impact ionization of the heavy atomic targets [47]. Furthermore, Dhankhar *et al.* [34] studied theoretically the double ionization of He atom in θ variable and constant θ_{12} mode for the twisted electron incidence. The same group also investigated the fivefold differential cross section (FDCS) and TDCS for the single ionization of molecular hydrogen (H_2). They also explored the influence of the twisted electron beam on the (e, 2e) process on the H_2 molecule from the perspective of the Young-type interference of the scattered waves emanating from the two atomic centers of the H_2 molecule. Their results found that the angular profile of the TDCS and FDCS depends on the OAM number, m, and the opening angle, θ_p, of the incident twisted electron beam [35].

To our knowledge, the investigations on electron impact ionization by twisted electron beams to date have been performed for single ionization of the hydrogenlike target atoms and H_2 molecule. In this paper, we present a theoretical estimation for the ionization of water molecule for the twisted electron beam. Our study is performed within the first Born approximation framework for an incident plane wave electron beam and for an incident twisted electron beam. We describe the plane wave, Slater-type wave functions, Coulomb wave for the scattered electron, the molecular state of H_2O, and the ejected electron, respectively.

In this paper, we take ejected electron energy small (8 eV and 10 eV) as compared to the energies of incident and scattered electron. This requires us to take into account properly the correlation between slow ejected electron and the multicenter complex target (here H_2O), which strongly affects the scattering dynamics. Even with the most advanced theoretical methods [14,20], there are certain discrepancies reported between the theory and experiment. Our model does not take into account the correlation effects due to the distorting potential of the ion the way it is taken into account in much more. sophisticated multicenter theoretical models. As mentioned earlier, the aim of the present study is to give a theoretical estimation for the twisted electron impact (e, 2e) process ionization on H_2O molecule. Certainly, there are better theoretical models for the plane wave (e, 2e) on H_2O and other multicenter targets, which can be explored in the future for the twisted electron (e, 2e) on H_2O.

In Secs. II A and II B, we present the theoretical formalism for the computation of the TDCS for the plane wave impact and twisted electron impact respectively. We present our results of the TDCS for the outer orbitals, namely, $1b_1$, $1b_2$, $3a_1$, and $2a_1$, of the water molecule for different parameters of the twisted electron beam in Sec. III. Finally, we conclude our paper in the Sec. IV. Atomic units are used throughout the paper unless otherwise stated.

II. THEORETICAL FORMALISM

This section presents the theoretical formalism for the computation of (e, 2e) differential cross sections of a water molecule for both the plane wave and the twisted electron beam as an incident beam. The (e, 2e) process on a water molecule can be described as;

$$e_i^- + H_2O \rightarrow e_s^- + e_e^- + H_2O^+ \tag{1}$$

here, e_i^-, e_s^-, and e_e^- represent the incident, scattered, and ejected electron, respectively. Figure 1 depicts the (e, 2e) process on H_2O molecule by plane wave electron beam in co-planar asymmetric geometry.

In the present theory, we apply the closure relation over all the possible rotational and vibrational states of the residual target (H_2O^+ ion). Thus the electron impact ionization of water molecule considered here is a pure electronic transition. We have neglected the exchange effects between the incident or scattered and bound or ejected electron since the incident or scattered electron is faster than the bound or ejected electron for the energies considered here [14].

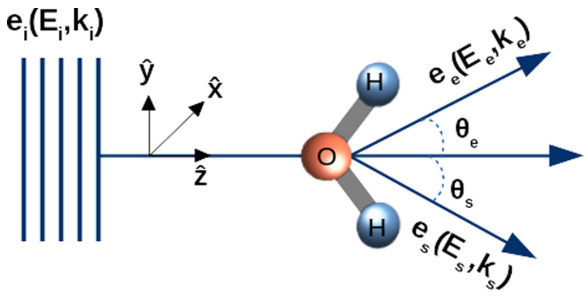

FIG. 1. Schematic diagram for the electron impact ionization of H_2O molecule, centered at oxygen nucleus, by plane wave in coplanar asymmetric geometry. An incident plane wave of energy E_i and momentum $\mathbf{k}_i$ interacts with the H_2O molecule ejecting one of the bound electrons of the molecule into continuum state. We describe E_s and E_e and $\mathbf{k}_s$ and $\mathbf{k}_e$ as the energies and momenta of the scattered and ejected electron, respectively. θ_s and θ_e represent the angular positions of the scattered and ejected electrons. The z axis is chosen along the propagation direction of the plane wave. The scattering plane is the xz plane and the scattered and ejected electrons are detected in scattering plane ($E_s > E_e$).

A. Plane wave ionization cross sections

For an (e, 2e) process on H_2O molecule, the fivefold differential cross section (5DCS) of a molecular orbital is given by [17],

$$\sigma^{(5)}(\alpha,\beta,\gamma) = \frac{d^5\sigma}{d\omega d\Omega_e d\Omega_s dE_e} = (2\pi)^4 \frac{k_e k_s}{k_i} \left|T_{fi}^{pw}\right|^2, \tag{2}$$

where $d\omega = \sin\beta d\alpha d\beta d\gamma$ is the solid angle element for the molecular orientation in the laboratory frame and α, β, and γ are the Euler angles of the water molecule. dE_e describes the energy interval for the ejected electron and $d\Omega_s$ and $d\Omega_e$ are the solid angle's intervals of the scattered and the ejected electron, respectively. $\mathbf{k_i}$, $\mathbf{k_s}$, and $\mathbf{k_e}$ represents the momentum of the incident, scattered and ejected electron, respectively. The scattering amplitude, T_{fi}^{pw}, describing the transition from the initial state ψ_i to final state ψ_f for a plane wave (in the first Born approximation) is given by,

$$T_{fi}^{pw} = \langle\psi_f|V|\psi_i\rangle, \tag{3}$$

where V describes the interaction between the incident electron and the molecular H_2O target and is given by;

$$V = \frac{-8}{r_0} - \frac{1}{|\mathbf{r}_0 - \mathbf{R}_{OH_1}|} - \frac{1}{|\mathbf{r}_0 - \mathbf{R}_{OH_2}|} + \sum_{i=1}^{10} \frac{1}{|\mathbf{r}_0 - \mathbf{r}_i|}, \tag{4}$$

where $\mathbf{R}_{OH_1}$ and $\mathbf{R}_{OH_2}$ represent the position vector of the two hydrogen nuclei from the oxygen nucleus with $|R_{OH_1}| = |R_{OH_2}| = 1.814$ a.u.. $\mathbf{r}_i$ is the position vector of the ith bound electron of the target with respect to the center of the oxygen nucleus (assumed to be fixed) and $\mathbf{r_0}$ is the position vector of the incident particle [22].

We develop the theoretical formalism with the following assumptions;

(1) Both the incident and the scattered electrons are described as a plane wave.

(2) The molecular wave function, $\Phi_j(\mathbf{r})$, is expressed as the linear combinations of the Slater-type functions centered at oxygen nucleus (self-consistent field LCAO [48]).

(3) The ejected electron is described by a Coulomb wave function, $\psi_{\mathbf{k}_e}^-(\mathbf{r})$.

(4) The exchange effects between the incident or scattered electron with the bound/ejected electron are neglected here since the incident/scattered electron is faster than the bound or ejected electron.

The electronic structure of water molecule consists of ten bound electrons, which are distributed among five one-center molecular orbitals expressed by linear combination of atomic orbitals (LCAO). The orbitals are $1b_1$, $3a_1$, $1b_2$, $2a_1$, and $1a_1$. The LCAO of each molecular orbital is characterized by a dominant atomic orbital component. The orbital $1b_1$ has $2p_{+1}$, $3a_1$ has $2p_0$, $1b_2$ has $2p_{-1}$, $2a_1$ has $2s$, and $1a_1$ has $1s$ dominant atomic orbital component [49]. The molecular orbitals expressed by the linear combinations of the Slater-type functions are given as (we follow the same mathematical representation as in Ref. [14]);

$$\Phi_j(\mathbf{r}) = \sum_{k=1}^{N_j} a_{jk} \phi_{n_{jk} l_{jk} m_{jk}}^{\xi_{jk}}(\mathbf{r}), \tag{5}$$

where N_j is the number of Slater functions used to describe the jth molecular orbital and n_{jk}, l_{jk}, m_{jk} are the quantum numbers for the jth molecular orbital. a_{jk} is the weight of each atomic component $\phi_{n_{jk} l_{jk} m_{jk}}^{\xi_{jk}}(\mathbf{r})$ and ξ_{jk} is a variational parameter. $\phi_{n_{jk} l_{jk} m_{jk}}^{\xi_{jk}}(\mathbf{r})$ is expressed as [50];

$$\phi_{n_{jk} l_{jk} m_{jk}}^{\xi_{jk}}(\mathbf{r}) = R_{n_{jk}}^{\xi_{jk}}(r) S_{l_{jk} m_{jk}}(\hat{\mathbf{r}}), \tag{6}$$

where $R_{n_{jk}}^{\xi_{jk}}(r)$ is the radial part of each atomic orbital and given as;

$$R_{n_{jk}}^{\xi_{jk}}(r) = \frac{(2\xi_{jk})^{n_{jk}+\frac{1}{2}}}{\sqrt{2n_{jk}!}} r^{n_{jk}-1} e^{-\xi_{jk} r}, \tag{7}$$

and $S_{l_{jk} m_{jk}}(\hat{\mathbf{r}})$ is the real spherical harmonics expressed as [51], with $m_{jk} \neq 0$:

$$S_{l_{jk} m_{jk}}(\hat{\mathbf{r}}) = \sqrt{\left(\frac{m_{jk}}{2|m_{jk}|}\right)} \Big\{ Y_{l_{jk}-|m_{jk}|}(\hat{\mathbf{r}}) + (-1)_{jk}^{m} \left(\frac{m_{jk}}{|m_{jk}|}\right) Y_{l_{jk}|m_{jk}|}(\hat{\mathbf{r}}) \Big\}, \tag{8}$$

and

$$m_{jk} = 0 : S_{l_{jk}0}(\hat{\mathbf{r}}) = Y_{l_{jk}0}(\hat{\mathbf{r}}). \tag{9}$$

Here $Y_{lm}(\hat{\mathbf{r}})$ is the complex spherical harmonics. The linear combination of spherical harmonics can be used for the transformation of the molecular orientation from the molecular frame to the laboratory frame expressed as [16]:

$$S_{lm}(\hat{\mathbf{r}}) = \sum_{\mu=-l}^{l} D_{m\mu}^{(l)}(\alpha,\beta,\gamma) S_{l\mu}(\hat{\mathbf{r}}), \tag{10}$$

where $D_{m\mu}^{(l)}(\alpha,\beta,\gamma)$ is the rotation matrix with Euler angles α, β and γ.

The problem of $N(=10)$ electrons can be reduced to one active electron problem using the frozen-core approximation. Within the framework of an independent electron approximation, it is assumed that one of the target electrons (the active one) is ejected in the final channel of the reaction, whereas the other electrons (the passive electrons) remain as frozen in their initial sates [17,52]. Performing the integration over $\mathbf{r}_0$ analytically (see Ref. [53]), we have,

$$\int \frac{e^{i\mathbf{K}\cdot\mathbf{r}_0}}{|\mathbf{r}_0-\mathbf{r}_1|}d^3r_0 = \frac{4\pi}{K^2}e^{i\mathbf{K}\cdot\mathbf{r}_1}. \tag{11}$$

The matrix element T_{fi} is thus given by,

$$T_{fi}^{pw}(\mathbf{q}) = \frac{-2}{q^2}\langle\psi_{\mathbf{k}_e}^{-}|e^{i\mathbf{q}\cdot\mathbf{r}}-1|\Phi_j(\mathbf{r})\rangle, \tag{12}$$

where $\mathbf{q}=\mathbf{k}_i-\mathbf{k}_s$ is the momentum transferred to the target. Here, $\psi_{\mathbf{k}_e}^{-}(\mathbf{r})$ and $\Phi_j(\mathbf{r})$ represent the Coulomb wave function and the molecular wave function, respectively.

For the gas-phase ionization of the water molecule, experimentally it is not possible to align the molecule in one particular orientation. Thus we compute the triple differential cross section (TDCS) by taking an average over all the possible orientations of the water molecule. We obtain the TDCS by integrating 5DCS over the Euler's angle and is given by;

$$\sigma^{(3)} = \frac{d^3\sigma}{d\Omega_e d\Omega_s dE_e} = \frac{1}{8\pi^2}\int \sigma^{(5)}(\alpha,\beta,\gamma)\sin\beta d\alpha d\beta d\gamma. \tag{13}$$

The integration over the Euler angles can then be performed using the ortho-normalization property of the rotation matrix and the TDCS is then given by [16],

$$\frac{d^3\sigma}{d\Omega_e d\Omega_s dE_e} = \frac{k_e k_s}{k_i}\sum_{k=1}^{N_j}\frac{a_{jk}^2}{\hat{l}_{jk}}\sum_{\mu=-l_{jk}}^{l_{jk}}\left|T_{fi}^{pw}(\mathbf{q})\right|^2, \tag{14}$$

where $\hat{l}_{jk}=2l_{jk}+1$.

B. Twisted electron ionization cross-sections

Figure 2 illustrates the (e, 2e) process on H_2O molecule by the twisted electron beam. A twisted electron beam is characterized by a helical wave front that twists around the beam axis as the beam propagates along the propagation direction. We use the same formalism as mentioned in Sec. II A, for the computation of the TDCS, except here we replace the plane wave function for the incident electron with a twisted electron wave function, such as a Bessel beam [42].

For an incident twisted electron beam, the momentum vector $\mathbf{k}_i$, can be described as [34],

$$\mathbf{k}_i = (k_i\sin\theta_p\cos\phi_p)\hat{x} + (k_i\sin\theta_p\sin\phi_p)\hat{y} + (k_i\cos\theta_p)\hat{z}, \tag{15}$$

where θ_p and ϕ_p are the polar and azimuthal angles of the $\mathbf{k}_i$, respectively. The longitudinal momentum is along the z axis. The momentum vector, $\mathbf{k}_i$, forms the surface of a cone with an angle θ_p with the z axis, which is normally referred as the opening angle of the twisted beam. $\theta_p=\tan^{-1}\frac{k_{i\perp}}{k_{iz}}$ with $k_{i\perp}$ and k_{iz} are the perpendicular and the longitudinal components of the momentum $\mathbf{k}_i$, respectively.

Experimentally it is difficult to obtain an exact alignment of the incident Bessel beam with the target, therefore, one needs

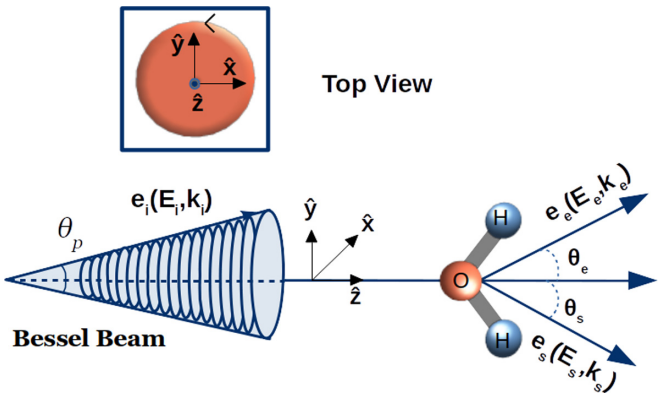

FIG. 2. Same as Fig. 1, except the incident beam is the twisted electron beam with an opening angle θ_p and OAM number "m". The quantization (z) axis is chosen along the propagation direction of the incoming beam. The inset represents the top view of the incident twisted electron beam. The beam propagates out of the page and twists around the propagation direction (counterclockwise).

to consider the Bessel beam with nonzero impact parameter ($\mathbf{b}$). This gives a more generalized equation for the Bessel beam [43] (which can be then be used to compute the TDCS for a macroscopic target by taking an average over all the possible impact parameters), such that

$$\psi_{\varkappa m}^{(tw)}(\mathbf{r}_0) = \int_0^\infty \frac{dk_{i\perp}}{2\pi}\,k_{i\perp}\int_0^{2\pi}\frac{d\phi_p}{2\pi}\,a_{\varkappa m}(\mathbf{k}_{i\perp})e^{i\mathbf{k}_i\cdot\mathbf{r}_0}e^{-i\mathbf{k}_i\cdot\mathbf{b}}, \tag{16}$$

where $a_{\varkappa m}(\mathbf{k}_{i\perp})=(-i)^m e^{im\phi_p}\delta(|\mathbf{k}_{i\perp}|-\varkappa)$ and $\varkappa$ is the absolute value of the transverse momentum $[k_i\sin(\theta_p)]$. $\mathbf{b}$ is the vector that describes the transverse orientation of the incident twisted electron beam with respect to the target. The impact parameter vector $\mathbf{b}$ is described as $\mathbf{b}=b\cos\phi_b\hat{x}+b\sin\phi_b\hat{y}$, with b as the magnitude of $\mathbf{b}$ and ϕ_b as the azimuthal angle of $\mathbf{b}$. In contrast to plane wave, the additional factor $e^{-i\mathbf{k}_i\cdot\mathbf{b}}$ in Eq. (16), implies the complex spatial structure of the Bessel beam [43].

By substituting the plane wave function with the Bessel wave function [Eq. (16) with Eq. (3)], we obtain the twisted wave transition amplitude $[T_{fi}^{tw}(\varkappa,\mathbf{q})]$ in terms of the plane wave transition amplitude $T_{fi}(\mathbf{q})$ [Eq. (12)] as (in the frozen-core approximation) [35];

$$T_{fi}^{tw}(\varkappa,\mathbf{q},\mathbf{b}) = (-i)^m\int_0^{2\pi}\frac{d\phi_p}{2\pi}\,e^{im\phi_p-i\mathbf{k}_{i\perp}\cdot\mathbf{b}}\,T_{fi}^{pw}(\mathbf{q}), \tag{17}$$

where, $\mathbf{k}_{i\perp}\cdot\mathbf{b}=\varkappa b\cos(\phi_p-\phi_b)$. The momentum transfer to the target for a twisted electron beam case can be expressed as;

$$q^2 = k_i^2+k_s^2-2k_ik_s\cos\theta, \tag{18}$$

where,

$$\cos\theta = \cos\theta_p\cos\theta_s+\sin\theta_p\sin\theta_s\cos(\phi_p-\phi_s). \tag{19}$$

In the above equation θ_s and ϕ_s are the polar and azimuthal angles of the $\mathbf{k}_s$. For the coplanar geometry $\phi_s=0$.

Here, the molecular target is assumed to be located along the direction of the incident twisted electron beam (z axis). Thus by using $\mathbf{b}=0$ in Eq. (17), the twisted wave transition

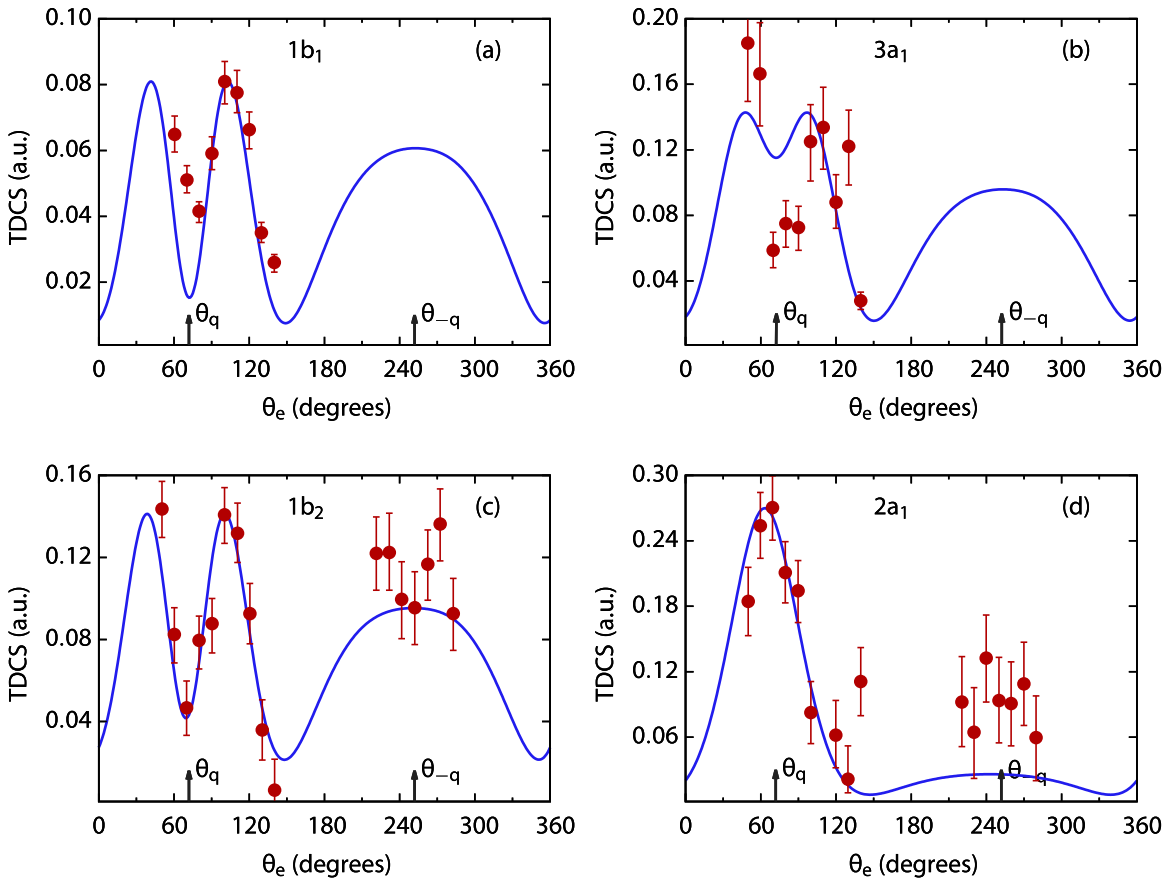

FIG. 3. TDCS as a function of ejected electron angle θ_e for the plane wave (e, 2e) process on H_2O molecule in the coplanar asymmetric geometry. Our plane wave results are represented by solid line and experimental results [54] by full circles. The kinematics used here is: $E_i = 250$ eV, $E_e = 10$ eV (except 8 eV for $3a_1$ orbital [(b)] and $\theta_s = 15^\circ$. Arrows indicate the direction of momentum transfer ($\theta_{\mathbf{q}}$) and recoil direction ($\theta_{-\mathbf{q}}$) [opposite to ($\theta_{\mathbf{q}}$) direction] for this and all subsequent figures.

amplitude $T_{fi}^{tw}(\varkappa, \mathbf{q})$, can be written as,

$$T_{fi}^{tw}(\varkappa, \mathbf{q}) = (-i)^m \int \frac{d\phi_p}{2\pi} e^{im\phi_p} T_{fi}^{pw}(\mathbf{q}). \tag{20}$$

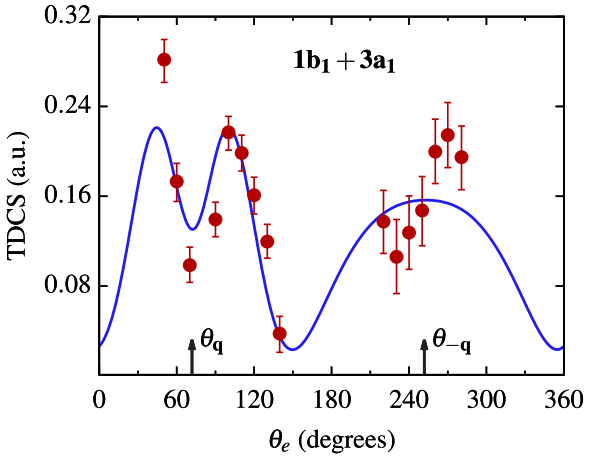

FIG. 4. Same as Fig. 3, except the summed TDCSs of the $1b_1$ and $3a_1$ orbitals are plotted. Kinematics is same as mentioned in Fig. 3

The TDCS for the molecular orbital of water molecule by twisted electron can be computed from Eq. (18) together with the transition amplitude $T_{fi}^{pw}(\mathbf{q})$ from the Eq. (12).

The process of ionization of a single molecule by a vortex beam is challenging experimentally. Therefore, in a more realistic scenario the ionization process on a macroscopic target is preferable [55]. The cross section for such a target can then be computed by taking the average of the plane wave cross sections over all the possible impact parameters, **b**, in the transverse plane of the twisted electron beam. The average cross section, $(\text{TDCS})_{av} = \overline{\frac{d^3\sigma}{d\Omega_s d\Omega_e dE_e}}$ in terms of plane wave cross section can be described as (for detailed derivation see Refs. [33,43,45]);

$$(\text{TDCS})_{av} = \frac{1}{2\pi \cos\theta_p} \int_0^{2\pi} d\phi_p \frac{d^3\sigma(\mathbf{q})}{d\Omega_s d\Omega_e dE_e}, \tag{21}$$

where $\frac{d^3\sigma(\mathbf{q})}{d\Omega_s d\Omega_e dE_e}$ is like the TDCS for the plane wave electron beam depending on $\mathbf{q}$. From Eq. (21), it is evident that the cross section for the scattering of the twisted electrons by the macroscopic target is independent of the OAM number m of the incident twisted electron beam. However, $(\text{TDCS})_{av}$ depends on the opening angle θ_p of the incident twisted electron beam.

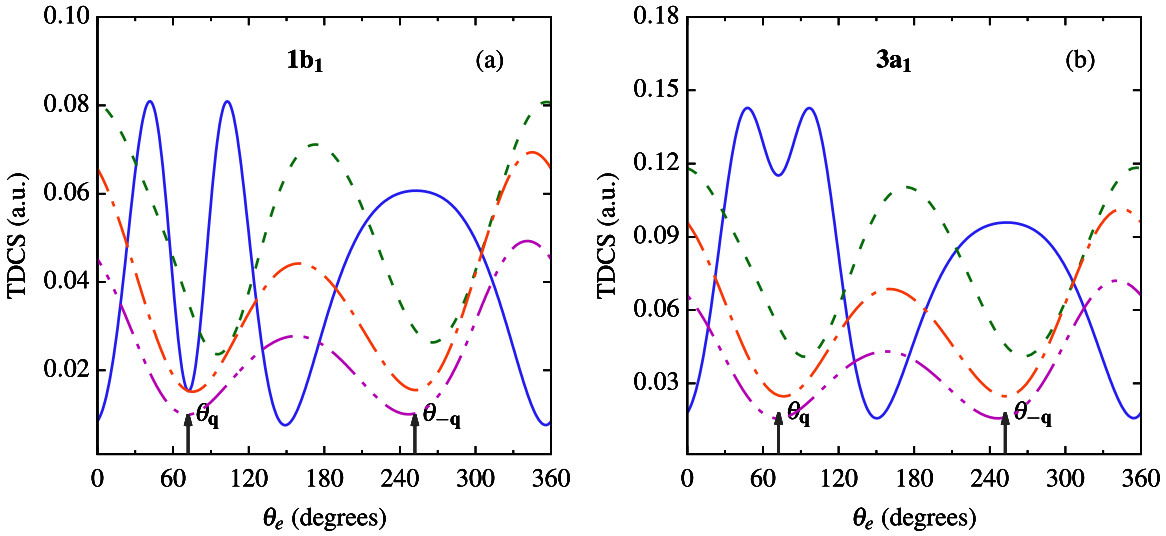

FIG. 5. TDCS as a function of ejection angle θ_e for the twisted electron wave (e, 2e) process on H_2O molecule in the coplanar asymmetric geometry. The kinematical conditions are $E_i = 250$ eV, $E_e = 10$ eV (except 8 eV for $3a_1$ orbital [(b)] and $\theta_p = \theta_s = 15^\circ$. The solid, dashed, dashed-dotted, and dashed-dotted-dotted curves represent the plane wave, $m = 1$, 2, and 3 respectively. The results for $m \neq 0$ are scaled up by a factor of 2 for both (a) and (b)

III. RESULTS AND DISCUSSIONS

In this section, we present the results of our calculations of the TDCS for H_2O by a twisted electron beam. We benchmark our theoretical results with the existing experimental data for the plane wave. We study the effect of different parameters of the twisted electron beam on the angular profiles of (e, 2e) cross sections for different orbitals of the water molecule. We present the single ionization differential cross section for the water molecule averaged over orientation in the gaseous phase. We compare our twisted electron beam results with that of plane wave results for different values of orbital angular momentum (OAM) number m, *viz.* 1, 2, and 3. The kinematics we have used here is; incident energy (E_i) = 250 eV, ejected energy (E_e) = 10 eV (except for the $3a_1$ molecular orbital for which $E_e = 8$ eV), $\theta_s = 15^\circ$ in the coplanar asymmetric geometry, similar to Milne-Brownlie *et al.* [54] for the plane wave (e, 2e) process. Since, experimentally, it is difficult to align the molecule in a particular direction, we compute the TDCS here.

A. Angular profiles of the TDCS for plane wave

We present in Fig. 3 the results of our calculations of the TDCS as a function of the ejected electron's angle (θ_e) for the plane wave electron beam in the coplanar asymmetric geometry for the outer orbitals of the water molecule, namely, $1b_1$, $3a_1$, $1b_2$, and $2a_1$. The arrows in the Fig. 3 and subsequent figures represent the direction of momentum transfer ($\theta_\mathbf{q}$) and the recoil direction ($\theta_{-\mathbf{q}}$). We compare the results of our calculation of the TDCS with the experimental data reported by Milne-Brownlie *et al.* [54] to benchmark our calculations so that we can validate our theoretical calculations for the twisted electron beam. The molecular wave function for the different orbitals of the water molecule is constructed from the linear combination of atomic orbitals (LCAO). Thus, the overall behavior of the TDCSs depend on the primary atomic component of each molecular orbital. As mentioned earlier, the $1b_1$ orbital's character is essentially dictated by a $2p_{+1}$ atomic orbital, the $3a_1$ by $2p_0$, the $1b_2$ by $2p_{-1}$ and the $2a_1$ by $2s$ [49,56,57]. For the present kinematics, the ionization process reveals these features in the angular distribution of the TDCS vs. θ_e. The two-peak structure around the binary region and the single peak in the recoil region for the orbitals $1b_1$, $1b_2$, and $3a_1$ is due to the strong p-like character of the orbitals [see Figs. 3(a)–3(c)]. While, due to the atomic s-like character of the $2a_1$ orbital, the binary peak is present along the momentum transfer direction and recoil peak along the recoil direction [17,49]. From Fig. 3, we observe that our theoretical model reproduces the experimental results quite well.

In Fig. 4, we present the angular profile for the summed contributions from the individual $1b_1$ and $3a_1$ orbitals since, due to low-energy resolution, the experiments are not able to resolve the peaks, particularly in the recoil region [54]. The two-peak structure demonstrates the atomic p-like character associated with both the orbitals. Our theoretical calculation reproduces the angular profile in the binary region quite well. However, it underestimates in the recoil region, which may be attributed to our simple theoretical model. Since the experimental results are on a relative scale, we have normalized them to compare the results with our theoretical results in the binary peak region. So, finally we conclude this section that the overall agreement between the plane wave experimental data and our theoretical data is good enough for the validity of our results for the twisted electron beam being presented in Sec. III B.

B. Angular profiles of the TDCS for twisted electron wave

In this section, we present the results of our calculation of the TDCS with the twisted electron beam for $E_i = 250$ eV, $E_e = 10$ eV (8 eV for $3a_1$ orbital) and $\theta_s = 15^\circ$ in the coplanar asymmetric geometrical mode. Here, we keep $\theta_p = \theta_s$

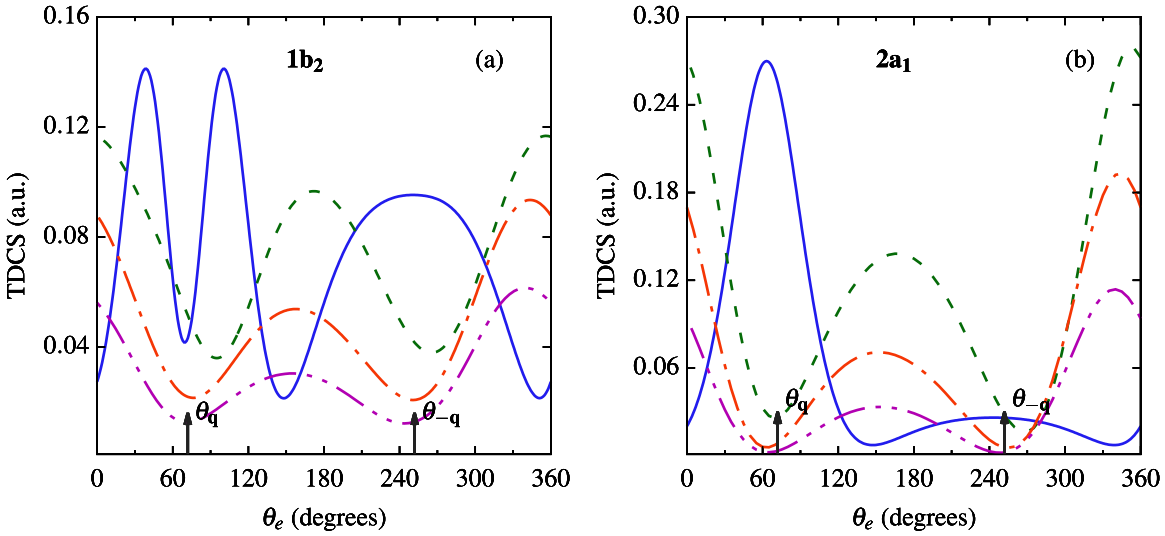

FIG. 6. Same as Fig. 5, except here for both the $1b_2$ and $2a_1$ orbitals and $E_e = 10$ eV. The results for $m \neq 0$ are scaled up by a factor of 2 in (a) and by 10 in (b).

and vary the OAM number m from 1–3 in a step of 1. In Figs. 5–7, the blue solid, green dashed, orange dashed-dotted, and magenta dashed-dotted-dotted curves represent the results for plane wave, $m = 1$, 2, and 3, respectively. Figures 5(a) and 5(b) represent the TDCS for the $1b_1$ and $3a_1$ orbitals, while Figs. 6(a) and 6(b) represent that for the $1b_2$ and $2a_1$ orbitals, respectively. As can be seen from the Figs. 5 and 6, the magnitude of the TDCS for $m \neq 0$ is reduced when compared with the $m = 0$ (the plane wave calculation). We have multiplied the results for all m for $1b_1$, $1b_2$, $3a_1$ orbitals by a factor of 2 and by a factor of 10 for $2a_1$ orbital. The magnitude further reduces when we gradually increase m up to 3 (see magenta dashed-dotted-dotted curve in Figs. 5 and 6).

For the p dominant orbitals, i.e., $1b_1$, $1b_2$, $3a_1$, we observe that the two-peak structure around the binary region disappears for all m [see dashed, dashed-dotted and dashed-dotted-dotted curves in the region marked by arrow in the binary region in Figs. 5(a), 5(b) and 6(a)]. Since the twisted electron beam represents a superposition of plane waves, no single momentum transfer is associated with the beam. The momentum transfer vector now has both longitudinal and transverse components. Also, the phase of the twisted electron beam depends on the OAM number m. The phase of the incident twisted electron beam varies with different values of m. Thus, due to the additional transverse component of the incident momentum vector and the OAM number dependence, the two-peak structure, as observed for the plane wave, disappears for the twisted electron case [33]. The twisted electron ionization studies by Harris *et al.* [33] and Dhankhar and Choubisa [35] showed the similar kind of OAM dependence on the angular profiles of the cross sections for the incident twisted electron beam. For the three orbitals, we observe a prominent contribution in the TDCS in the forward and backward direction for $m = 1$, 2, and 3 [see peaks around $\theta_e = 0°$ (360°) and 180° for dashed, dashed-dotted and dashed-dotted-dotted curves]. For the $2a_1$ orbital, for $m = 1$, 2, and 3 we observe substantial contribution in the forward and backward regions [see peaks around $\theta_e = 0°$ (360°) and 180° for dashed, dashed-dotted, and dashed-dotted-dotted curves in Fig. 6(b)]. In both Figs. 5 and 6, we observe a minimum at or around the plane wave linear momentum transfer direction (see dashed, dashed-dotted, and dashed-dotted-dotted curves in Figs. 5 and 6 around the arrows). Due to an additional transverse momentum component in the incident momentum for the twisted electron beam, the peaks observed for the plane wave case are shifted significantly for the twisted electron case.

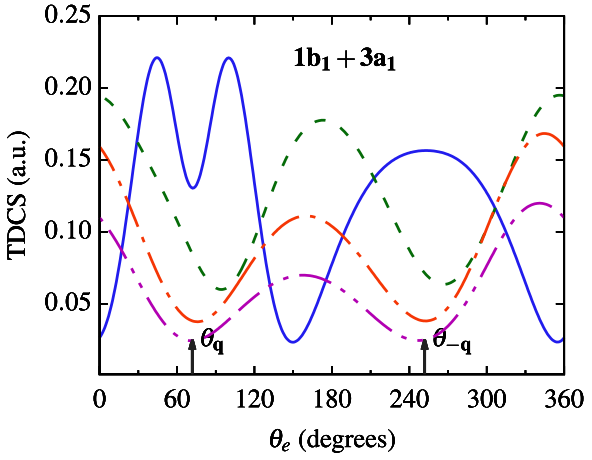

FIG. 7. Summed TDCS of the $1b_1$ and $3a_1$ orbitals as a function of ejection angle θ_e for a twisted electron beam. Kinematics is same as mentioned in Fig. 3. The magnitude of the TDCS for $m \neq 0$ is scaled up by a factor of 2.

In Fig. 7, we present the angular profiles of TDCS for the summed contributions of the $1b_1$ and $3a_1$ orbitals as a function of ejected electron angle θ_e for the twisted electron beam. The two-peak structure, as observed for the plane wave, disappears for the twisted electron beam as well. We also observe peaks in the forward and backward direction (see peaks around $\theta_e = 0°$ and 180°) as observed in the earlier cases. We have scaled up our calculations for the twisted electron beam by a factor of 2. We found that with an increasing m, the magnitude of the TDCS decreases. In Figs. 5–7, we observe

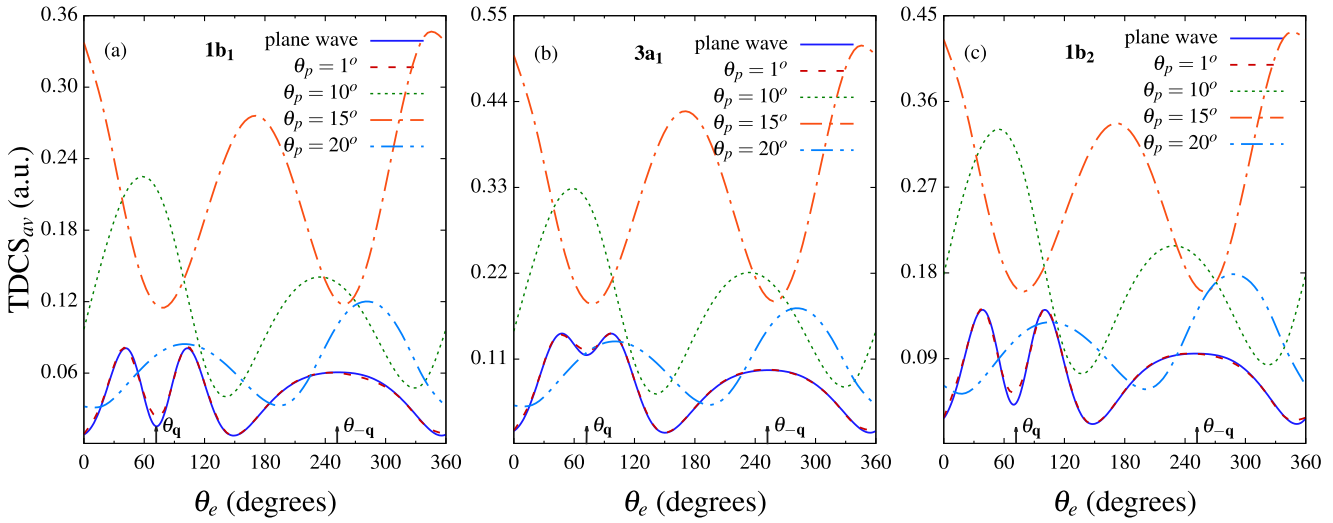

FIG. 8. $(\text{TDCS})_{av}$ plotted as a function of the ejected electron angle θ_e for the plane wave (solid line) and twisted electron beam for different opening angles as shown in the frames of each subfigure. The kinematics is same as used in Figs. 5 and 6.

that for an increasing OAM number m, the ratio of forward to backward peak increases. For example, for the $1b_1$ orbital the ratio of the forward peak to backward peak for m =1, 2, and 3 is 1.126, 1.568, and 1.775, respectively [see dashed, dashed-dotted and dashed-dotted-dotted curves in Fig. 5(a)]. Also, with an increasing m, both the forward and backward peaks shift towards the smaller angle (see dashed, dashed-dotted, and dashed-dotted-dotted curves around $\theta_e = 180^\circ$ in Figs. 5–7).

C. Angular profiles for the $(\text{TDCS})_{av}$ for a macroscopic H_2O molecular target

In Figs. 8 and 9, we present the results of our calculations for the TDCS averaged over the impact parameter **b**, $(\text{TDCS})_{av}$, for $1b_1$, $3a_1$, and $1b_2$ orbitals (Fig. 8) and for $2a_1$ orbital (Fig. 9), as a function of the ejected electron angle (θ_e). The $(\text{TDCS})_{av}$ depends on the opening angle θ_p of the incident twisted electron beam [see Eq. (21)]. Figures 8 and 9 represent

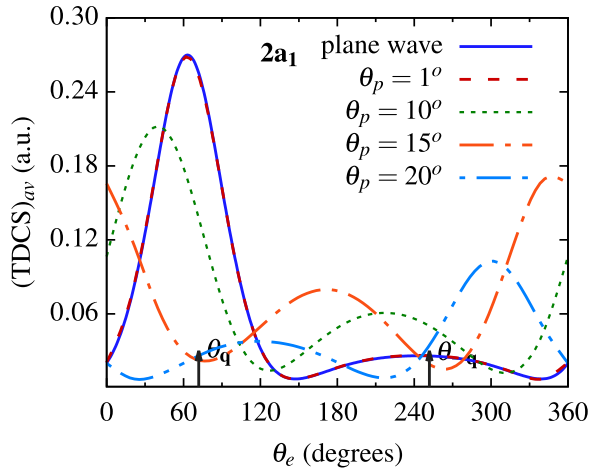

FIG. 9. Same as Fig. 8, except for the $2a_1$ orbital and $E_e = 10$ eV.

the $(\text{TDCS})_{av}$ for the kinematics $E_i = 250$ eV, $E_e = 10$ eV (8 eV for the $3a_1$ orbital) and $\theta_s = 15^\circ$. We present the angular profiles of the $(\text{TDCS})_{av}$ for $\theta_p = 1^\circ$, 10°, 15°, and 20° of the twisted electron beam and compare them with the plane wave angular profiles.

From Figs. 8 and 9, we observe that for a smaller opening angle, such as $\theta_p = 1^\circ$, the angular profile of the $(\text{TDCS})_{av}$ is similar to that of the plane wave for all the orbitals (see solid and dashed curves in Figs. 8 and 9). For $\theta_p = 10^\circ$, the characteristic two-peak structure in the binary region for the p-type orbitals ($1b_1$, $3a_1$, and $1b_2$) disappear and a broad single-peak structure appears with an enhanced magnitude as compared to the plane wave (see dotted curves in Fig. 8). For the s-type orbital $2a_1$, however, the binary-peak structure is maintained (see dotted curve in Fig. 9) and the magnitude of the $(\text{TDCS})_{av}$ is less than that for the plane wave. The recoil peak is, however, observed for all the orbitals for $\theta_p = 10^\circ$ (see dotted curve around $\theta_{-\mathbf{q}}$ in Figs. 8 and 9). We also observe that both the binary and recoil peaks are shifted from the plane wave momentum transfer direction (see dotted curves in Figs. 8 and 9). For the $\theta_p = \theta_s$ (15°) case, we observe prominent peaks in the forward and backward regions for all the orbitals [see dashed-dotted curves in Figs. 8 and 9 around $\theta_e = 0^\circ$ (or 360°) and 180°] with an enhanced magnitude of $(\text{TDCS})_{av}$ for the p-type orbitals only. For a larger opening angle, such as $\theta_p = 20^\circ$, we observe a two-peak structure in the angular profile of the $(\text{TDCS})_{av}$ for all the orbitals ($1b_1$, $1b_2$, $3a_1$, and $2a_1$) with prominent peak around recoil direction and a shallow peak in the binary direction. These two-peak structures are in contrast to the prominent binary-peak structure in the plane wave (see dashed-dotted-dotted curves in Figs. 8 and 9). For $\theta_p = 20^\circ$, the magnitude of the $(\text{TDCS})_{av}$ is higher than the plane wave for the p-type orbitals only, but less than those for the $\theta_p = 10^\circ$ and 15° (see dashed-dotted-dotte curves in Fig. 8). Hence, it is clear that the average cross section depends on the opening angle θ_p.

In order to understand the angular profiles of $(\text{TDCS})_{(av)}$ for the different orbitals of the water molecule, we plot the

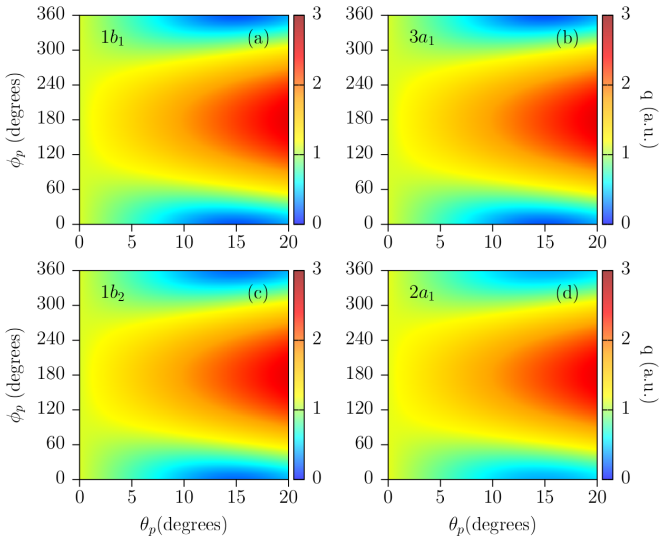

FIG. 10. Magnitude of the momentum transfer as a function of the opening angle (θ_p) and azimuthal angle (ϕ_p). The kinematics is kept same as for Fig. 3.

momentum transfer as a function of opening and azimuthal angles (θ_p and ϕ_p) of the twisted electron beam [see Eq. (18)] in Fig. 10. From Eqs. (18) and (19), we see that the momentum transfer vector **q** for the twisted electron beam depends on both polar and azimuthal angles (θ_p and ϕ_p) of the incident beam. The momentum transfer for the twisted electron beam has both longitudinal and transverse components, in contrast to the plane wave. For a fixed opening angle, the transverse component of the momentum vector changes with each ϕ_p. From Fig. 10 we observe that for a fixed opening angle the magnitude of momentum transfer is minimum for $\phi_p = 0^\circ$ and maximum for $\phi_p = 180^\circ$. For the p-type orbitals $1b_1$, $3a_1$, and $1b_2$, the magnitude of momentum transfer is significantly small in the forward region around $\phi_p = 0^\circ$ at higher opening angles such as 10°, 15°, and 20° (see blue islands for $\phi_p = 0^\circ$ or 360° for $1b_1$, $3a_1$, and $1b_2$ around $\theta_p = \theta_s$ region in Fig. 10) when compared to the smaller opening angle such as 1°. These TDCSs, corresponding to the smaller momentum transfer, results in a shifting of the prominent peaks (for higher opening angles) and the enhancement of the magnitude of the $(\text{TDCS})_{av}$ (for the p-type orbitals only) than that for the plane wave. As elaborated in Ref. [32], in the computation of $(\text{TDCS})_{av}$, the cross-section contributions from the smaller momentum transfer magnitude dominate the average over ϕ_p. Since the $(\text{TDCS})_{av}$ can be described in terms of the plane wave cross section [see Eq. (21)]. We can deduce from Eqs. (12) and (21), that the plane wave cross section depends on the inverse power of the momentum transfer (q^{-4}) in the first Born approximation. As an integrand, we see that the plane wave TDCSs ($\frac{d^3\sigma(\mathbf{q})}{d\Omega_s d\Omega_e dE_e}$) dominates for the smaller **q** in the computation of the $(\text{TDCS})_{av}$ [see Eq. (21)]. This is evident from the angular profiles of the $1b_1$, $3a_1$ and $1b_2$ orbitals in Fig. 8 [see islands of low **q** in the forward region in Figs. 10(a)–10(c)].

However, for the $2a_1$ orbital, we observe that the magnitude of the prominent peak decreases with an increasing opening angle (θ_p) (see dashed, dotted, dashed-dotted, and dashed-dotted-dotted curves in Fig. 9). The decrease in the magnitude of the prominent peak (when compared with the p-type orbitals) with an increase in opening angle can be explained by the fact that for the $2a_1$ orbital, the low momentum transfer islands (as notable for the p-type orbitals) are not that pronounced [see Fig. 10(d)]. As a result, the smaller momentum transfer TDCSs have comparatively less dominance in the computation of the $(\text{TDCS})_{av}$ for the $2a_1$ orbital. The results of the averaged cross section for the $2a_1$ orbital are also consistent with those for the twisted electron (e, 2e) results of the H atom by Harris *et al.* (2019) (s-type orbital) [33].

IV. CONCLUSION

In this paper, we have presented the theoretical study of the triple-differential cross sections (TDCS) for an (e, 2e) process on H_2O molecule by the twisted electron beam. We studied the angular distributions of the TDCS for the coplanar asymmetric geometry in the first Born approximation for both the plane and twisted electron beam. We have studied the effect of the OAM number, m, on the TDCS for $m = 1$, 2, and 3. We have benchmarked our theoretical results with the experimental data for the plane wave electron beam. For the (e, 2e) ionization of the H_2O by twisted electron impact, we observe that for the $1b_1$, $3a_1$, and $1b_2$ orbitals (exhibiting atomic p-type orbital characteristics), the two-peak structures in the binary region, which is the signature of the p-type atomic orbital, disappear. For the $2a_1$ orbital (governed by an atomic s-type orbital) the peaks in the binary and recoil region are no longer present. We observe peaks in the forward and backward direction for all the outer orbitals in contrast to their plane wave ionization cross-section profiles. Due to the dependence on the additional transverse momentum and the OAM number m of the incident twisted electron beam, the angular profiles of the TDCS for the twisted electron case are different from the plane wave profiles. Our results show that the magnitude of the cross section is minimum around the plane wave momentum transfer direction for the different m. We also observed that with an increasing value of the OAM number m, the magnitude of the TDCS decreases. We also discuss the $(\text{TDCS})_{av}$ (averaged over the impact parameter **b**) as a function of the opening angle θ_p of the twisted electron beam. For a macroscopic target, the angular profiles of $(\text{TDCS})_{av}$ significantly depend on the opening angle (θ_p) of the twisted electron beam.

Our present paper is an attempt to investigate the (e, 2e) process on the H_2O molecule to unravel the effects of the twisted electron's different parameters on the angular profile of the TDCS. We have used the 1CW wave function in our theoretical model to study the TDCS. The present study can also be extended for other molecular targets, such as N_2, NH_3, CH_4, etc. Besides this, one can further explore the differential cross sections going beyond the first Born approximation. We present here comprehensive research on the (e, 2e) processes on the H_2O molecule for the twisted electrons. Hence, our findings in this work must be taken from that perspective. We are confident that the present work will help to progress theoretical and experimental research in this

subject. The present study can be further extended for a twisted electron beam impact ionization using more sophisticated models, such as DWBA, 2CW, BBK, and DS3C, in the near future [14,19–21].

ACKNOWLEDGMENTS

The authors acknowledge Didier Sébilleau for his valuable cooperation in the work.

[1] R. I. Campeanu, H. R. J. Walters, and C. T. Whelan, Phys. Rev. A **97**, 062702 (2018).
[2] C. T. Whelan, H. Walters, A. Lahmam-Bennani, and H. Ehrhardt, *(e, 2e) & Related Processes* (Springer Science & Business Media, Berlin, 2012), Vol. 414.
[3] J. Colgan, M. S. Pindzola, F. J. Robicheaux, D. C. Griffin, and M. Baertschy, Phys. Rev. A **65**, 042721 (2002).
[4] A. Lahmam-Bennani, A. Naja, E. M. S. Casagrande, N. Okumus, C. D. Cappello, I. Charpentier, and S. Houamer, J. Phys. B: At., Mol. Opt. Phys. **42**, 165201 (2009).
[5] O. Al-Hagan, *Theoretical Study of Electron Impact-Ionization of Molecules* (Missouri University of Science and Technology, Rolla, 2010).
[6] X. Ren, S. Amami, O. Zatsarinny, T. Pflüger, M. Weyland, W. Y. Baek, H. Rabus, K. Bartschat, D. Madison, and A. Dorn, Phys. Rev. A **91**, 032707 (2015).
[7] L. Mouawad, P. A. Hervieux, C. D. Cappello, J. Pansanel, A. Osman, M. Khalil, and Z. E. Bitar, J. Phys. B: At., Mol. Opt. Phys. **50**, 215204 (2017).
[8] T. Khatir, S. Houamer, and C. D. Cappello, J. Phys. B: At., Mol. Opt. Phys. **52**, 245201 (2019).
[9] G. Purohit, Atoms **9**, 31 (2021).
[10] A. I. Lozano, F. Costa, X. Ren, A. Dorn, L. Álvarez, F. Blanco, P. Limão-Vieira, and G. García, Int. J. Mol. Sci. **22**, 4601 (2021).
[11] B. Boudaıffa, P. Cloutier, D. Hunting, M. A. Huels, and L. Sanche, Science **287**, 1658 (2000).
[12] M. Blanc, D. Andrews, A. Coates, D. Hamilton, C. Jackman, X. Jia, A. Kotova, M. Morooka, H. Smith, and J. Westlake, Space Sci. Rev. **192**, 237 (2015).
[13] E. Alizadeh, T. M. Orlando, and L. Sanche, Annu. Rev. Phys. Chem. **66**, 379 (2015).
[14] C. Champion, C. Dal Cappello, S. Houamer, and A. Mansouri, Phys. Rev. A **73**, 012717 (2006).
[15] C. Champion, Phys. Med. Biol. **55**, 11 (2009).
[16] M. Sahlaoui and M. Bouamoud, Can. J. Phys. **89**, 723 (2011).
[17] M. L. de Sanctis, M.-F. Politis, R. Vuilleumier, C. R. Stia, and O. A. Fojón, J. Phys. B: At., Mol. Opt. Phys. **48**, 155201 (2015).
[18] C. M. G. Castro, Ph.D. thesis, Université de Lorraine, 2016.
[19] X. Ren, S. Amami, K. Hossen, E. Ali, C. G. Ning, J. Colgan, D. Madison, and A. Dorn, Phys. Rev. A **95**, 022701 (2017).
[20] M. Gong, X. Li, S. B. Zhang, S. Niu, X. Ren, E. Wang, A. Dorn, and X. Chen, Phys. Rev. A **98**, 042710 (2018).
[21] P. Singh, G. Purohit, C. Champion, D. Sébilleau, and D. Madison, J. Chem. Phys. **150**, 054304 (2019).
[22] C. Champion, D. Oubaziz, H. Aouchiche, Y. V. Popov, and C. Dal Cappello, Phys. Rev. A **81**, 032704 (2010).
[23] D. B. Jones, M. Yamazaki, N. Watanabe, and M. Takahashi, Phys. Rev. A **83**, 012704 (2011).
[24] D. Oubaziz, M. A. Quinto, and C. Champion, Phys. Rev. A **91**, 022703 (2015).
[25] M. Uchida and A. Tonomura, Nature (London) **464**, 737 (2010).
[26] J. Verbeeck, H. Tian, and P. Schattschneider, Nature (London) **467**, 301 (2010).
[27] B. J. McMorran, A. Agrawal, I. M. Anderson, A. A. Herzing, H. J. Lezec, J. J. McClelland, and J. Unguris, Science **331**, 192 (2011).
[28] S. M. Lloyd, M. Babiker, G. Thirunavukkarasu, and J. Yuan, Rev. Mod. Phys. **89**, 035004 (2017).
[29] K. Bliokh, I. Ivanov, G. Guzzinati, L. Clark, R. V. Boxem, A. Béché, R. Juchtmans, M. Alonso, P. Schattschneider, F. Nori, and J. Verbeeck, Phys. Rep. **690**, 1 (2017).
[30] H. Larocque, I. Kaminer, V. Grillo, G. Leuchs, M. J. Padgett, R. W. Boyd, M. Segev, and E. Karimi, Contemp. Phys. **59**, 126 (2018).
[31] A. Asenjo-Garcia and F. J. García de Abajo, Phys. Rev. Lett. **113**, 066102 (2014).
[32] A. Plumadore and A. L. Harris, J. Phys. B: At., Mol. Opt. Phys. **53**, 205205 (2020).
[33] A. L. Harris, A. Plumadore, and Z. Smozhanyk, J. Phys. B: At., Mol. Opt. Phys. **52**, 094001 (2019).
[34] N. Dhankhar, A. Mandal, and R. Choubisa, J. Phys. B: At., Mol. Opt. Phys. **53**, 155203 (2020).
[35] N. Dhankhar and R. Choubisa, J. Phys. B: At., Mol. Opt. Phys. **54**, 015203 (2020).
[36] R. Juchtmans, A. Béché, A. Abakumov, M. Batuk, and J. Verbeeck, Phys. Rev. B **91**, 094112 (2015).
[37] X. Qiu, F. Li, W. Zhang, Z. Zhu, and L. Chen, Optica **5**, 208 (2018).
[38] A. S. Maxwell, G. S. J. Armstrong, M. F. Ciappina, E. Pisanty, Y. Kang, A. C. Brown, M. Lewenstein, and C. Figueira de Morisson Faria, Faraday Discuss. **228**, 394 (2021).
[39] R. Van Boxem, Ph.D. thesis, Universiteit Antwerpen, 2016.
[40] I. P. Ivanov and V. G. Serbo, Phys. Rev. A **84**, 033804 (2011).
[41] R. Van Boxem, B. Partoens, and J. Verbeeck, Phys. Rev. A **89**, 032715 (2014).
[42] R. Van Boxem, B. Partoens, and J. Verbeeck, Phys. Rev. A **91**, 032703 (2015).
[43] V. Serbo, I. P. Ivanov, S. Fritzsche, D. Seipt, and A. Surzhykov, Phys. Rev. A **92**, 012705 (2015).
[44] M. Schüler and J. Berakdar, Phys. Rev. A **94**, 052710 (2016).
[45] D. V. Karlovets, G. L. Kotkin, V. G. Serbo, and A. Surzhykov, Phys. Rev. A **95**, 032703 (2017).
[46] A. V. Maiorova, S. Fritzsche, R. A. Müller, and A. Surzhykov, Phys. Rev. A **98**, 042701 (2018).
[47] A. Mandal, N. Dhankhar, D. Sébilleau, and R. Choubisa, Phys. Rev. A **104**, 052818 (2021).

[48] R. Moccia, J. Chem. Phys. **40**, 2186 (1964).
[49] C. Champion, J. Hanssen, and P. A. Hervieux, Phys. Rev. A **63**, 052720 (2001).
[50] C. Champion, J. Hanssen, and P. A. Hervieux, Phys. Rev. A **72**, 059906(E) (2005).
[51] T. Helgaker, P. Jorgensen, and J. Olsen, *Molecular Electronic-Structure Theory* (John Wiley & Sons, New York, 2014).
[52] M. Sahlaoui and M. Bouamoud, J. Phys. B: At., Mol. Opt. Phys. **45**, 085201 (2012).
[53] R. Tweed, Z. Phys. D **23**, 309 (1992).
[54] D. S. Milne-Brownlie, S. J. Cavanagh, B. Lohmann, C. Champion, P. A. Hervieux, and J. Hanssen, Phys. Rev. A **69**, 032701 (2004).
[55] V. A. Zaytsev, A. Surzhykov, V. G. Serbo, V. P. Kosheleva, M. E. Groshev, V. A. Yerokhin, V. M. Shabaev, and T. Stöhlker, J. Phys.: Conf. Ser. **1412**, 052013 (2020).
[56] H. Hafid, B. Joulakian, and C. D. Cappello, J. Phys. B: At., Mol. Opt. Phys. **26**, 3415 (1993).
[57] J. Hanssen, B. Joulakian, C. D. Cappello, and H. Hafid, J. Phys. B: At., Mol. Opt. Phys. **27**, 3547 (1994).